INTERFACE SHEAR STRENGTH OF COMPOSITE CONCRETE-TO-CONCRETE BOND

MAZIZAH EZDIANI BT MOHAMAD

A thesis submitted in fulfilment of the

requirements for the award of the degree of

Doctor of Philosophy (Civil Engineering)

Faculty of Civil Engineering

Universiti Teknologi Malaysia

AUGUST 2016

Dedicated to

my family and friends

ACKNOWLEDGEMENTS

I wish to express my sincere appreciation to my main thesis supervisor, Dr. Izni Syahrizal Bin Ibrahim, for motivations, guidance, critics and full academic support. Without his continued support and interest, this thesis would not have been the same as presented here.

I am greatly indebted to Universiti Teknologi Malaysia (UTM) for given me this golden opportunity to pursue Ph.D., most especially; School of Graduate Studies, Faculty of Civil Engineering, Department of Materials and Structure, Sultanah Zanariah Library and Technicians-Structural, Materials laboratory UTM and Computational Mechanics Solid Laboratory, Faculty of Mechanical Engineering.

I gratefully acknowledge the support to all my family members and friends.

ABSTRACT

Interface shear strength between two concrete layers cast at different times plays an important role to develop composite action of the floor slabs. Most previous studies when quantifying interface shear strength for interface concrete with projecting steel did not take concrete cohesion into consideration. In contrast, interface concrete without projecting steel depended solely on concrete cohesion in quantifying the interface shear strength. Although there are studies conducted on the action of interface shear strength under variable normal stresses, the findings only considered smooth or left “as-cast” surface. Furthermore, Finite Element Modeling (FEM) of the interface shear behavior for concrete-to-concrete bond is also limited in research. In this study, a total of 72 “push-off” tests were carried out to study the interface shear strength of composite slab with six different surface textures. This included smooth or left “as-cast”, roughened by wire-brushing in the longitudinal and transverse direction, groove, indented and projecting steel crossing the interface. Loading was then applied horizontally on the concrete topping until failure was observed under various normal stresses; σ_n = 0 N/mm^2, 0.5 N/mm^2, 1.0 N/mm^2 and 1.5 N/mm^2. The relationship between surface texture, interface shear strength and normal stress was then proposed in this study. The roughness profile of the concrete base was measured using a portable stylus roughness instrument. The experimental results show that the transverse roughened surface produced the highest interface shear strength of 1.89 N/mm^2 (at σ_n = 0 N/mm^2), 4.69 N/mm^2 (at σ_n = 0.5 N/mm^2), 5.97 N/mm^2 (at σ_n = 1.0 N/mm^2) and 6.42 N/mm^2 (at σ_n = 1.5 N/mm^2). This is then followed by roughened in the longitudinal direction, indented, groove and smooth or left “as-cast” surfaces. The increase in the degree of roughness contributed to higher concrete cohesion and friction coefficient. The surface with projecting steel exhibited plastic deformation and yielding before it failed completely as compared with the other surfaces which failed in brittle fracture. Analytical equations were then proposed to predict the friction coefficient and concrete cohesion by integrating R_{pm} into the interface shear strength equation for surface without projecting steel. In contrast, for surface with projecting steel, the proposed design equation does not integrate R_{pm} in determining friction coefficient and concrete cohesion. The comparison shows good concordance with the experimental results within an acceptable range. The results from the “push-off” test were then compared and validated with Finite Element Analysis (FEA) using Cohesive Zone Model (CZM). The percentage differences between the FEA model and the proposed analytical equations ranged from 6% to 29% (smooth or “left as-cast”), 4% to 14% (indented), 3% to 21% (transverse roughened) and 58% to 72% (surface with projecting steel). In addition, the interface shear strength properties from the “push-off” FEA results were applied in the full-scale composite slab FEA modeling. The composite slab was modeled using Concrete Damaged Plasticity (CDP) for smooth or left “as-cast”, indented and transverse roughened surfaces. Meanwhile, the surface with projecting steel was modeled using Cap Plasticity Model (CPM). The study concluded that the design interface shear strength, v_{Rdi} from the proposed equation of the “push-off” test should be higher than the interface shear strength, v_{Edi} based on the ultimate vertical shear load of the full-scale FEA model. As stated in Eurocode 2, the actual interface shear strength should be lower or equal to the design value ($v_{Edi} \leq v_{Rdi}$) for the composite slab to act monolithically.

ABSTRAK

Kekuatan ricih antara muka dua lapisan konkrit dituang pada masa yang berlainan memainkan peranan penting untuk menghasilkan tindakan komposit papak lantai. Kebanyakan kajian sebelumnya apabila mengukur kekuatan ricih konkrit antara muka dengan unjuran keluli tidak mengambil kira paduan konkrit. Sebaliknya, konkrit antara muka tanpa unjuran keluli bergantung sepenuhnya kepada paduan konkrit dalam mengukur kekuatan ricih antara muka. Walaupun terdapat kajian dijalankan ke atas tindakan kekuatan ricih antara muka dengan tegasan normal pelbagai, bagaimanapun, penemuan tersebut hanya mengambil kira permukaan licin atau "as-cast". Tambahan pula, Model Unsur Terhingga (FEM) untuk ikatan konkrit-ke-konkrit terhadap kelakuan ricih antara muka juga terhad dalam penyelidikan. Dalam kajian ini, sebanyak 72 ujian "push-off" telah dijalankan untuk mengkaji kekuatan ricih antara muka papak komposit dengan enam jenis tekstur permukaan. Ini termasuk licin atau "as-cast", kasar dengan berus dawai dalam arah membujur dan melintang, keluk alur, lekukan dan unjuran keluli melintasi antara muka. Beban kemudiannya dikenakan secara melintang terhadap penutup konkrit sehingga kegagalan diperolehi di bawah kepelbagaian tegasan normal; 0 N/mm^2, 0.5 N/mm^2, 1.0 N/mm^2 dan 1.5 N/mm^2. Hubungan di antara tekstur permukaan, kekuatan ricih antara muka dan tegasan normal dicadangkan dalam kajian ini. Profil kekasaran asas konkrit diukur dengan menggunakan alat kekasaran "stylus" mudah alih. Keputusan eksperimen menunjukkan bahawa permukaan kasar melintang menghasilkan kekuatan ricih antara muka paling tinggi iaitu 1.89 N/mm^2 (σ_n = 0 N/mm^2), 4.69 N/mm^2 (σ_n = 0.5 N/mm^2), 5.97 N/mm^2 (σ_n = 1.0 N/mm^2) dan 6.42 N/mm^2 (σ_n = 1.5 N/mm^2). Ia kemudiannya diikuti dengan permukaan kasar membujur, lekukan, keluk alur dan licin atau "as-cast". Peningkatan terhadap tahap kekasaran menyumbang kepada paduan konkrit dan pekali geseran yang tinggi. Permukaan dengan unjuran keluli mempamerkan ubah bentuk plastik dan alah sebelum gagal sepenuhnya jika dibandingkan dengan permukaan lain yang gagal dalam patah rapuh. Persamaan analitikal dicadangkan untuk meramalkan pekali geseran dan paduan konkrit dengan mengintegrasikan R_{pm} ke dalam persamaan kekuatan ricih antara muka untuk permukaan tanpa unjuran keluli. Sebaliknya, untuk permukaan dengan unjuran keluli, persamaan rekabentuk yang dicadangkan tidak mengintegrasikan R_{pm} dalam menentukan pekali geseran dan paduan konkrit. Perbandingan menunjukkan persetujuan yang baik dengan julat yang boleh diterima. Keputusan daripada ujian "push-off" kemudiannya dibandingkan dan disahkan dengan Analisis Unsur Terhingga (FEA) menggunakan Cohesive Zon Model (CZM). Peratus perbezaan di antara model FEA dengan persamaan analitikal yang dicadangkan adalah dalam julat 6% hingga 29% (licin atau "as-cast"), 4% hingga 14% (lekukan), 3% kepada 21% (kasar melintang) dan 58% kepada 72% (permukaan dengan unjuran keluli). Di samping itu, ciri-ciri kekuatan ricih antara muka daripada keputusan FEA "push-off" telah diaplikasikan di dalam model FEA papak komposit berskala penuh. Papak komposit dimodelkan dengan menggunakan Concrete Damaged Plasticity (CDP) di permukaan licin atau "as-cast", keluk alur dan kasar melintang. Sementara itu, permukaan dengan unjuran keluli dimodelkan menggunakan Cap Plasticity Model (CPM). Kesimpulannya, kekuatan ricih antara muka, v_{Rdi} daripada cadangan persamaan ujian "push-off" perlu lebih tinggi daripada kekuatan ricih antara muka, v_{Edi} berdasarkan beban ricih muktamad menegak model FEA berskala penuh. Seperti yang dinyatakan di dalam Eurocode 2, kekuatan ricih antara muka sebenar haruslah lebih rendah atau sama dengan nilai rekabentuk, $v_{Edi} \leq v_{Rdi}$ untuk papak komposit bertindak secara monolitik.

TABLE OF CONTENTS

CHAPTER	TITLE		PAGE
	DECLARATION		ii
	DEDICATION		iii
	ACKNOWLEDGEMENT		iv
	ABSTRACT		v
	ABSTRAK		vi
	TABLE OF CONTENTS		vii
	LIST OF TABLES		xiv
	LIST OF FIGURES		xvii
	LIST OF SYMBOLS		xxix
	LIST OF ABBREVIATIONS		xxxiv
	LIST OF APPENDICES		xxxv
1	**INTRODUCTION**		**1**
	1.1	Introduction	1
	1.2	Problem Statement	3
	1.3	Objectives	5
	1.4	Scope of Study	6
	1.5	Significant of Study	7
	1.6	Thesis Organization	8

2	**LITERATURE REVIEW**		**10**
	2.1	Introduction	10
	2.2	Shear Transfer Mechanism at Interface	10
		2.2.1 Shear-Friction Theory	11
		2.2.2 Cohesion-plus-Shear Friction	15
	2.3	Shear Transfer across Interface of Different Ages	17
		2.3.1 Interfacial Behavior	18
		2.3.2 Relationship Between Interface Shear Stress and Normal Stress	25
		2.3.3 Concrete Strength	28
	2.4	Surface Roughness	32
		2.4.1 Interface Shear Strength	35
	2.5	Previous Work of Composite Members	43
		2.5.1 Precast Girder Beam and Concrete Topping	44
		2.5.2 Hollow Core Slab (HCS) and Concrete Topping	47
	2.6	International Codes of Practice on Interface Shear Strength	48
		2.6.1 Eurocode 2 (2004)	49
		2.6.2 ACI 318 (2008)	50
		2.6.3 CEB-FIP Model Code 2010	52
		2.6.4 Comparison between the Design Expressions	53
	2.7	Finite Element Modeling	56
		2.7.1 The Finite Element Code ABAQUS	57
		2.7.2 Cohesive Zone Modeling	58
		2.7.3 Modified Drucker-Prager/Cap Plasticity Model	60
		2.7.4 “Push-off” Test Model	62

2.8 Summary 64

3 EXPERIMENTAL WORK 66

3.1 Introduction 66
3.2 Specimen Description 69
3.3 Method of Specimen Preparation 72
3.4 Curing 76
3.5 Surface Roughness Quantification 77
3.5.1 Roughness Instrument 78
3.5.2 Method of Roughness Measurement 79
3.5.3 Roughness Parameter 79
3.6 "Push-off" Test Setup 82
3.7 Summary 84

4 FINITE ELEMENT MODELING 86

4.1 Introduction 86
4.2 Cohesive Zone Model (CZM) 87
4.2.1 CZM for Interface Concrete without Projecting Steel 87
4.3 Interface Concrete with the Projecting Steel 91
4.4 FEM Procedure for Small-Scale Model 93
4.4.1 Specimen Description 93
4.4.2 Finite Element Mesh 97
4.4.3 Interaction 99
4.4.4 Boundary Condition 101
4.4.5 Loading 104
4.5 FEM Procedure for Full-Scale Model 105

	4.5.1	Concrete Material Model	105
		4.5.1.1 Interface Concrete without Projecting Steel	105
		4.5.1.2 Interface Concrete with Projecting Steel	111
	4.5.2	Steel Material Model	112
	4.5.3	Specimen Description	113
	4.5.4	Finite Element Mesh	117
	4.5.5	Interaction	118
	4.5.6	Boundary Condition	119
	4.5.7	Loading	121
4.6		Summary	121

5 EXPERIMENTAL RESULTS AND DISCUSSION 123

5.1		Introduction	123
5.2		Concrete Strength Test Results	124
5.3		Surface Texture Profile	124
5.4		Interface Failure Mode	127
	5.4.1	Interface Concrete without Projecting Steel	127
	5.4.2	Interface Concrete with Projecting Steel	131
5.5		Horizontal Load-Interface Slip Relationship	132
5.6		Interface Shear Strength	146
	5.6.1	Interface Shear Strength – Roughness Parameter Relationship at Interface Concrete without Projecting Steel	146
	5.6.2	Interface Shear Strength at Interface Concrete with Projecting Steel	153
5.7		Coefficient of Correlation for Roughness Parameters and Pre-crack Interface Shear Strength	154

	5.8	Friction Coefficient and Concrete Cohesion	156
		5.8.1 Determination of Friction Coefficient and Concrete Cohesion at Interface Concrete without the Projecting Steel by Roughness Parameter	156
		5.8.2 Determination of Friction Coefficient and Concrete Cohesion at Interface Concrete with the Projecting Steel	162
		5.8.3 Comparison between Interface Concrete with and without the Projecting Steel	162
	5.9	Comparison and Discussion with the Experimental Results	164
		5.9.1 Comparison of Friction Coefficient and Concrete Cohesion at Interface Concrete without the Projecting Steel by Roughness Parameter	165
		5.9.2 Comparison of Interface Shear Strength	167
		5.9.3 Comparison with the Codes of Practice	171
		5.9.4 Comparison of Design Expression between Previous Researchers and Current Study	178
	5.10	Summary	185
6	**RESULTS AND DISCUSSION: SMALL-SCALE FINITE ELEMENT MODELING**		**188**
	6.1	Introduction	188
	6.2	Finite Element Mesh Sensitivity Analysis	188
	6.3	FE Modeling Results of the Interface Concrete without Projecting Steel	194
		6.3.1 FE Modeling Results for Smooth or Left “as-cast” Surface	195
		6.3.1.1 Stress Distribution Diagram	195

6.3.1.2 Horizontal Load-Interface Slip Relationship 201

6.3.2 FE Modeling Results for Indented Surface 202

6.3.2.1 Stress Distribution Diagram 203

6.3.2.2 Horizontal Load-Interface Slip Relationship 208

6.3.3 FE Modeling Results for Transverse Roughened Surface 209

6.3.3.1 Stress Distribution Diagram 210

6.3.3.2 Horizontal Load-Interface Slip Relationship 215

6.4 FE Modeling Results of the Interface Concrete with Projecting Steel 216

6.4.1 Stress Distribution Diagram 218

6.4.2 Horizontal Load-Interface Slip Relationship 223

6.5 Interface Shear Stress Distribution Analysis 225

6.5.1 Smooth or Left “as-cast” Surface 225

6.5.2 Indented Surface 227

6.5.3 Transverse Roughened Surface 229

6.5.4 Surface with Projecting Steel 232

6.6 Interface Shear Strength 233

6.7 Summary 235

7 RESULTS AND DISCUSSIONS: FULL-SCALE FINITE ELEMENT MODELING 237

7.1 Introduction 237

7.2 FE Model Test Results of the Full-Scale Composite Slab 238

7.2.1 Applied Load-Deflection Relationship 241

		7.2.2	Ultimate Shear Capacity	245
		7.2.3	Verification of the Composite Slab FE Model	246
		7.2.4	Stress Distribution in the Composite Slab FE Model	250
		7.2.5	Interface Shear Stress Distribution Analysis	255
	7.3	Interface Shear Strength		257
		7.3.1	Comparison with Design Equations Proposed by Previous Research	262
	7.4	Summary		265
8	**CONCLUSION**			**267**
	8.1	Conclusions		262
		8.1.1	Interface shear strength of composite slab with different surface textures	268
		8.1.2	Relationship between interface shear strength and friction coefficient, concrete cohesion, normal stress and clamping stress from projecting steel	268
		8.1.3	The interface shear strength of Finite Element Modeling on the composite slab with different surface textures and comparison with the experimental results	269
		8.1.4	Relationship between the interface shear strength and the shear capacity of the full scale composite slab from the Finite Element Modeling	270
	8.2	Recommendations for Further Investigations		271
REFERENCES				**273**
Appendices A-E				280

LIST OF TABLES

TABLE NO.	TITLE	PAGE
2.1	Correlation between Interface Shear Strength and Roughness Parameter	41
2.2	Friction coefficient and concrete cohesion according to Eurocode 2	50
2.3	Friction coefficient proposed by ACI 318	51
2.4	Friction and cohesion coefficients according to CEB-FIP Model Code 2010	52
2.5	Interface shear strength for various established Codes of Practice	54
3.1	Specimen description	72
3.2	Mix design proportions for the concrete base and concrete topping	76
3.3	Roughness parameters	79
4.1	Cap plasticity concrete model parameters at interface	91
4.2	Finite element meshes for each surface texture	97
4.3	Modeling properties for small-scale specimen of interface concrete without projecting steel	98
4.4	Modeling properties for small-scale specimen of interface concrete with projecting steel	99
4.5	Concrete Damaged Plasticity (CDP) model parameters for concrete model	111
4.6	Cap Plasticity Model (CPM) parameters for concrete model	112

4.7	Finite element meshes for each surface texture	118
5.1	Test results on the concrete compressive strength and tensile strength	124
5.2	Summary of test results at σ_n = 0 N/mm^2	142
5.3	Summary of test results at σ_n = 0.5 N/mm^2	143
5.4	Summary of test results at σ_n = 1.0 N/mm^2	144
5.5	Summary of test results at σ_n = 1.5 N/mm^2	145
5.6	Summary roughness parameters at σ_n = 0 N/mm^2	149
5.7	Summary roughness parameters at σ_n = 0.5 N/mm^2	150
5.8	Summary roughness parameters at σ_n = 1.0 N/mm^2	151
5.9	Summary roughness parameters at σ_n = 1.5 N/mm^2	152
5.10	Coefficient of correlation, R^2, between roughness parameters and pre-crack interface shear strength	155
5.11	Comparison of friction coefficient between experimental, Eurocode 2 and Equation (5.3)	160
5.12	Comparison of concrete cohesion between experimental, Eurocode 2 and Equation (5.4)	161
5.13	Comparison between the experimental results and Eurocode 2	164
5.14	Experimental and calculated interface shear strength using the proposed concrete cohesion, *c* and friction coefficient, μ	170
5.15	Comparison of Design Expression, Friction and Cohesion Coefficient between Codes of Practice and proposed design expression	172
5.16	Average roughness parameter of R_{pm} and R_a to calculate the interface shear strength	173
5.17	Comparison of the interface shear strength between the experimental and the design values in Eurocode 2 (2004), ACI 318 (2008) and CEB-FIB Model Code 2010 (2010)	174
5.18	Summary of design expression proposed by previous Researchers	184

6.1	Interface properties for interface concrete without projecting steel	195
6.2	Interface properties for interface concrete with projecting steel	217
6.3	Comparison of the interface shear strength between the FE model results and the calculated values	234
7.1	Interface properties for interface concrete with and without projecting steel	241
7.2	Summary of the FE model shear test results	246
7.3	Comparison of the interface shear strength between the FE model results and the theoretical values	261
7.4	Comparison of the interface shear strength between the FE model and previous studies	264

LIST OF FIGURES

FIGURE NO.	TITLE	PAGE
1.1	Placing the precast slab	1
1.2	Composite action between existing precast slab and newly added concrete topping	2
1.3	Projecting steel at the top of the precast slab	4
1.4	Non-composite section (Kovach and Naito, 2008)	4
1.5	Composite section (Kovach and Naito, 2008)	5
2.1	Shear friction hypothesis proposed by Birkeland and Birkeland (1966)	13
2.2	Saw-tooth model (Santos and Júlio, 2012)	14
2.3	Mechanical concept of sliding	15
2.4	Coulomb's failure criterion	17
2.5	The "push-off" specimens by Hanson (1960)	18
2.6	Reproduced typical stress-slip curves from the "push-off" test by Hanson (1960)	19
2.7	Anderson's "push-off" test method (Anderson, 1960)	20
2.8	Reproduced horizontal shear data (Birkeland and Birkeland, 1966)	23
2.9	Direct shear test setup by Sonnenberg *et al.* (2003)	27
2.10	Reproduced interface shear strength influence on the concrete strength (Walraven et al., 1988)	29

2.11	Comparison between the interface shear strength equation before and after considering the concrete compressive strength	31
2.12	Comparison between design expressions of interface shear strength from previous studies considering the concrete compressive strength	32
2.13	Schematic diagram of portable stylus roughness instrument	34
2.14	Determination of center arithmetical mean line	34
2.15	Typical cross-section of a rib and block floor system tested by Gohnert (2003)	36
2.16	Basic dimensions of the composite members tested by Gohnert (2003)	36
2.17	Schematic diagram of the "push-off" test rig by Gohnert (2003)	37
2.18	Graphical representations of roughness measurement (Gohnert, 2003)	37
2.19	Reproduced relationship between interface shear strength and concrete compressive strength (Gohnert, 2003)	38
2.20	Reproduced relationship between interface shear strength and roughness parameter (Gohnert, 2003)	39
2.21	(a) Slant shear test setup and (b) Pull-off test specimen (Santos *et al*., 2007)	40
2.22	Typical detail of the test beams by Loov and Patnaik (1994)	44
2.23	Typical load-deflection curve for composite beam with smooth surface compared with the predicted behavior in ACI (Patnaik, 2001)	46
2.24	Beam cross section of Phase 2 test specimen (Kovach and Naito, 2008)	47
2.25	Detailed section of the test specimen by Scott (1973)	48
2.26	Indented surface recommended in Eurocode 2 (2004)	49

2.27	Comparison of interface shear strength with established Codes of Practice (ACI 318, 2008, Eurocode 2, 2004 and CEB-FIP Model Code 2010, 2010)	55
2.28	Cohesive zone models are embedded along connected meshes and describe the traction-separation relationship as a softening curve (Richefeu *et al.*, 2012)	58
2.29	Bilinear representation of CZM	60
2.30	Yield surfaces of the modified cap model in the *p*-*t* plane (Simulia, 2012)	61
2.31	Mesh study with two meshes size (a) 15 mm and (b) 5 mm and (c) normal and shear stress components along the interface for P_y =120 kN (Dias-da-Costa *et al.*, 2012)	63
2.32	Boundary study: (a) boundary conditions with zero-thickness elements in the lower plate; (b) scheme of the load cell ring in contact with the plate (Dias-da-Costa *et al.*, 2012)	64
3.1	Research methodology flowcharts	68
3.2	“Push-off” test specimen	69
3.3	Surface textures for the concrete base	71
3.4	Provision of mesh reinforcement of 6 mm diameter plain round mild steel bars in the concrete base and concrete topping	73
3.5	Preparation of the concrete base and concrete topping	74
3.6	Concrete cubes and cylinders	75
3.7	Burlaps used for wet curing	77
3.8	Portable stylus roughness instrument	78
3.9	“Push-off” test setup: a) Schematic drawing and b) Actual picture	83
3.10	Positioning of the load cell for the horizontal load application	84
3.11	Positioning of the load cell for the normal load application	84

4.1	Result of "push-off" test as a tool for validation of FEM simulation	88
4.2	Typical traction-separation responses	89
4.3	Penalty stiffness related to displacement at damage initiation in "push-off" test	89
4.4	Tensile stress-strain behavior for 6 mm diameter mild steel reinforcement embedded in concrete	92
4.5	Average stress-strain curve of steel bars embedded in concrete (Wang and Hsu, 2001)	93
4.6	"Push-off" specimen modeling	94
4.7	Smooth surface	95
4.8	Indented surface	95
4.9	Wire brushing in transverse direction surface	96
4.10	Projecting steel crossing the interface	96
4.11	Interface elements for smooth surface	99
4.12	Interface elements for indented surface	100
4.13	Interface elements for projecting steel crossing the interface	100
4.14	Cohesive failure obtained from the experimental test for wire-brushing in the transverse direction surface	101
4.15	The bottom section is fixed in the *x*-, *y*- and *z*-directions (U1 = U2 = U3 = UR1 = UR2 = UR3 = 0) at initial step	102
4.16	Side wall of the concrete base is restrained against movement in the *x*-direction (U1 = 0) at first step	102
4.17	Horizontal load application at concrete topping is restrained against movement in the *x*-direction (U1 = 0) at first step	103
4.18	Step by step process for the boundary conditions	103
4.19	Load applied using kinematic coupling constraint	104
4.20	Response of concrete to uniaxial loading in (a) tension and (b) compression (Simulia, 2012)	107

4.21	Family of hyperbolic flow potentials in the *p*-*q* plane	108
4.22	Stress-strain relationships for the concrete base (f_{cu} = 40 N/mm^2)	110
4.23	Tensile stress-strain relationships for the concrete base (f_{cu} = 40 N/mm^2)	110
4.24	Stress-strain relationships for the concrete topping (f_{cu} = 25 N/mm^2)	110
4.25	Tensile stress-strain relationships for the concrete topping (f_{cu} = 25 N/mm^2)	111
4.26	Stress-strain relationships for the concrete base (f_{cu} = 40 N/mm^2)	112
4.27	Stress-strain relationships for the concrete topping (f_{cu} = 25 N/mm^2)	112
4.28	Stress-strain relationships for 16 mm high tensile steel reinforcement	113
4.29	Stress-strain relationships for 6 mm diameter mild steel reinforcement	113
4.30	Configuration of the composite concrete slab	114
4.31	Composite slab; a) dimensional properties and b) the FEM modelling of the composite slab	115
4.32	Positioning the steel bar in the composite slab: a) 6 mm diameter steel bar at concrete topping, and b) 16 mm diameter steel bar at concrete base	116
4.33	Smooth surface	116
4.34	Indented surface	117
4.35	Wire-brushing in transverse direction surface	117
4.36	Projecting steel crossing the interface	117
4.37	Completed model of the composite slab using interface element as tied constraint and steel reinforcement as embedded constraint	119
4.38	Location of the roller and plate support in the composite slab	120

4.39	Boundary condition at the support	120
4.40	Boundary condition at mid-span of slab	120
5.1	Smooth or left "as-cast" surface	125
5.2	Groove surface	126
5.3	Indented surface	126
5.4	Wire-brushing roughened in longitudinal direction	126
5.5	Wire-brushing roughened in transverse direction	127
5.6	Failure mode of smooth surface: (a) failure plane along interface, and (b) adhesive failure at the interface	128
5.7	Failure mode of groove surface: (a) failure plane along interface, and (b) adhesive failure at the interface	128
5.8	Failure mode of indented surface: (a) failure plane along the interface, and (b) adhesive failure at the interface	129
5.9	Failure mode of the longitudinal roughened surface: (a) failure plane along interface, and (b) cohesive failure at the interface	130
5.10	Failure mode of transverse roughened surface: (a) failure plane along interface, and (b) cohesive failure at the interface	130
5.11	Failure mode of the surface with projecting steel: (a) failure plane along interface, (b) rear view with small chipping of the concrete topping, and (c) the exposed projecting steel which is deformed but still remained intact to both concretes	131
5.12	Horizontal load-interface slip relationship for smooth or "left as-cast" surface at: (a) σ_n = 0 N/mm^2, (b) σ_n = 0.5 N/mm^2, (c) σ_n = 1.0 N/mm^2, and (d) σ_n = 1.5 N/mm^2	136
5.13	Horizontal load-interface slip relationship for groove surface at: (a) σ_n = 0 N/mm^2, (b) σ_n = 0.5 N/mm^2, (c) σ_n = 1.0 N/mm^2, and (d) σ_n = 1.5 N/mm^2	137
5.14	Horizontal load-interface slip relationship for indented surface at: (a) σ_n = 0 N/mm^2, (b) σ_n = 0.5 N/mm^2, (c) σ_n = 1.0 N/mm^2, and (d) σ_n = 1.5 N/mm^2	138

5.15	Horizontal load-interface slip relationship for wire-brushing in longitudinal direction surface at: (a) σ_n = 0 N/mm^2, (b) σ_n = 0.5 N/mm^2, (c) σ_n = 1.0 N/mm^2, and (d) σ_n = 1.5 N/mm^2	139
5.16	Horizontal load-interface slip relationship for wire-brushing in transverse direction surface at: (a) σ_n = 0 N/mm^2, (b) σ_n = 0.5 N/mm^2, (c) σ_n = 1.0 N/mm^2, and (d) σ_n = 1.5 N/mm^2	140
5.17	Horizontal load-interface slip relationship for projecting steel surface at: a) σ_n = 0 N/mm^2, (b) σ_n = 0.5 N/mm^2, (c) σ_n = 1.0 N/mm^2, and (d) σ_n = 1.5 N/mm^2	141
5.18	Coefficient of correlation, R^2 between roughness parameters and pre-crack interface shear strength under four variables normal stresses	155
5.19	Mohr-Coulomb failure envelope of interface concrete without the projecting steel	157
5.20	Relationship between friction coefficient, concrete cohesion and mean peak height, R_{pm}	158
5.21	Mohr-Coulomb failure envelope of interface concrete with steel	162
5.22	Comparison between the experimental and calculated; a) concrete cohesion, b) friction coefficient	166
5.23	Comparison between the experimental and calculated interface shear strength	171
5.24	Comparison of interface shear strength from the “push-off” test between the experimental and theoretical for surfaces without projecting steel	176
5.25	Comparison of interface shear strength from the “push-off” between the experimental and theoretical for surface with projecting steel	177
5.26	Comparison of design expression from previous researchers and Code of Practice on smooth or left “as-cast” surface	180
5.27	Comparison of design expression from previous researchers and Code of Practice on deep groove surface	181

5.28	Comparison of design expression from previous researchers and Code of Practice on indented surface	181
5.29	Comparison of design expression from previous researchers and Code of Practice on longitudinal roughened surface	182
5.30	Comparison of design expression from previous researchers and Code of Practice on transverse roughened surface	182
5.31	Comparison of design expression from previous researchers and Code of Practice on surface provided with projecting steel	183
6.1	Sensitivity analysis using meshing sizes for smooth or left "as-cast" surface: (a) refined mesh (5 mm), (b) medium coarse mesh (15 mm), (c) coarse mesh (20 mm), and (d) horizontal load-interface slip relationships	190
6.2	Sensitivity analysis using meshing sizes for indented surface: (a) refined mesh (5 mm), (b) medium coarse mesh (15 mm), (c) coarse mesh (20 mm), and (d) horizontal load-interface slip relationships	191
6.3	Sensitivity analysis using meshing sizes for transverse roughened surface: (a) refined mesh (5 mm), (b) medium coarse mesh (15 mm), (c) coarse mesh (20 mm), and (d) horizontal load-interface slip relationships	192
6.4	Sensitivity analysis using meshing sizes for surface with projecting steel: (a) refined mesh (5 mm), (b) medium coarse mesh (15 mm), (c) coarse mesh (20 mm), and (d) horizontal load-interface slip relationships	193
6.5	Von Mises Stress distribution diagram for smooth or left "as-cast" surface at σ_n = 0 N/mm^2: (a) under the applied normal load, (b) peak shear load, and (c) interface shear failure	197
6.6	Von Mises Stress distribution diagram for smooth or left "as-cast" surface at σ_n =0.5 N/mm^2: (a) under the applied normal load, (b) peak shear load, and (c) interface shear failure	198

6.7	Von Mises Stress distribution diagram for smooth or left "as-cast" surface at σ_n = 1.0 N/mm^2: (a) under the applied normal load, (b) peak shear load, and (c) interface shear failure	199
6.8	Von Mises Stress distribution diagram for smooth or left "as-cast" surface at σ_n = 1.5 N/mm^2: (a) under the applied normal load, (b) at peak shear load, and (c) interface shear failure	200
6.9	Horizontal load-interface slip relationships for smooth or left "as-cast" surface	202
6.10	Von Mises Stress distribution diagram for indented surface at σ_n = 0 N/mm^2: (a) under the applied normal load, (b) at peak shear load, and (c) interface shear failure	204
6.11	Von Mises Stress distribution diagram for indented surface at σ_n = 0.5 N/mm^2: (a) under the applied normal load, (b) at peak shear load, and (c) interface shear failure	205
6.12	Von Mises Stress distribution diagram for indented surface at σ_n = 1.0 N/mm^2: (a) under the applied normal load, (b) at peak shear load, and (c) interface shear failure	206
6.13	Von Mises Stress distribution diagram for indented surface at σ_n = 1.5 N/mm^2: (a) under the applied normal load, (b) at peak shear load, and (c) interface shear failure	207
6.14	Horizontal load-interface slip relationships for indented surface	209
6.15	Von Mises Stress distribution diagram for transverse roughened surface at σ_n = 0 N/mm^2: (a) under the applied normal load, (b) at peak shear load, and (c) interface shear failure	211
6.16	Von Mises Stress distribution diagram for transverse roughened surface at σ_n = 0.5 N/mm^2: (a) under the applied normal load, (b) at peak shear load, and (c) interface shear failure	212
6.17	Von Mises Stress distribution diagram for transverse roughened surface at σ_n = 1.0 N/mm^2: (a) under the applied normal load, (b) at peak shear load, and (c) interface shear failure	213

6.18 Von Mises Stress distribution diagram for transverse roughened surface at σ_n = 1.5 N/mm^2: (a) under the applied normal load, (b) at peak shear load, and (c) interface shear failure 214

6.19 Horizontal load-interface slip relationships for transverse roughened surface 216

6.20 Von Mises Stress distribution diagram of the surface with projecting steel at σ_n = 0 N/mm^2: (a) normal load applied, (b) peak shear load, (c) interface shear failure, and (d) deformed shape of the projecting steel 219

6.21 Von Mises Stress distribution diagram of the surface with projecting steel at σ_n = 0.5 N/mm^2: (a) normal load applied, (b) peak shear load, (c) interface shear failure, and (d) deformed shape of the projecting steel 220

6.22 Von Mises Stress distribution diagram of the surface with projecting steel at σ_n = 1.0 N/mm^2: (a) normal load applied, (b) peak shear load, (c) interface shear failure, and (d) deformed shape of the projecting steel 221

6.23 Von Mises Stress distribution diagram of the surface with projecting steel at σ_n = 1.5 N/mm^2: (a) normal load applied, (b) peak shear load, (c) interface shear failure, and (d) deformed shape of the projecting steel. 222

6.24 Horizontal load-interface slip relationships for surface with projecting steel 224

6.25 Interface shear stress distributions at peak shear load for smooth or left "as-cast" surface: (a) nodes location at the interface, (b) σ_n = 0 N/mm^2, (c) σ_n = 0.5 N/mm^2, (d) σ_n = 1.0 N/mm^2, (e) σ_n = 1.5 N/mm^2, and (f) stress distribution along the interface length 226

6.26 Interface shear stress distributions at peak shear load for indented surface: (a) nodes location at the interface, (b) σ_n = 0 N/mm^2, (c) σ_n = 0.5 N/mm^2, (d) σ_n = 1.0 N/mm^2, (e) σ_n = 1.5 N/mm^2, and (f) stress distribution along the interface length 228

6.27	Interface shear stress distributions at peak shear load for transverse roughened surface: (a) nodes location at the interface, (b) σ_n = 0 N/mm^2, (c) σ_n = 0.5 N/mm^2, (d) σ_n = 1.0 N/mm^2, (e) σ_n = 1.5 N/mm^2, (f) interaction between the concrete layers, and (g) stress distribution along the interface length	230
6.28	Interface shear stress distributions at peak shear load for surface with projecting steel: (a) nodes location at the interface, (b) σ_n = 0 N/mm^2, (c) σ_n = 0.5 N/mm^2, (d) σ_n = 1.0 N/mm^2, (e) σ_n = 1.5 N/mm^2, and (f) stress distribution along the interface length	232
7.1	The location of nodal location to determine vertical deflection and interface slip	239
7.2	Total internal energy and kinetic energy versus time relationship of the full-scale FE model	240
7.3	Interface slip between the concrete layers	240
7.4	Shear load-deflection relationships for the various surface textures	243
7.5	Shear load-interface slip relationships for the various surface textures	245
7.6	Composite hollow core slab with interface element modeling approach (Mones, 2012)	247
7.7	Interface shear strength properties assigned to the interface elements in the direction resisting horizontal shear (Mones, 2012)	247
7.8	Stress distribution diagram following interface failure (Mones, 2012)	248
7.9	Load-deflection plots for composite slab at transversely broomed surface (Mones, 2012)	248
7.10	Small-scale testing (Joshani *et al.*, 2012)	249
7.11	Interface layer at concrete-to-steel interface (Joshani *et al.*, 2012)	249
7.12	Load-deflection plots from experimental and FE modeling of composite slab at concrete-to-steel bond (Joshani *et al.*, 2012)	250

7.13	Smooth or left "as-cast" surface at: (a) Von Mises stress contour, and (b) Tensile cracking damage	251
7.14	Indented surface at: (a) Von Mises stress contour, and (b) Tensile cracking damage	252
7.15	Transverse roughened surface at: (a) Von Mises stress contour, (b) Tensile cracking damage	253
7.16	Von Mises stress contour for the surface with projecting steel: (a) shear stress distribution following the interface shear failure, (b) stress contour under the loading plate, (c) stress contour under the slab, and (d) projecting steel deformed between the support and loading plate	254
7.17	Interface shear stress distributions at peak shear load at: (a) smooth or left "as-cast" surface, (b) indented surface, (c) transverse roughened, and (d) projecting steel surface	256
7.18	Interface shear stress distribution pattern for the various surface textures	257

LIST OF SYMBOLS

α	-	Angle of the inclination of the indentation
β	-	Ratio of the longitudinal force in the new concrete area and the total longitudinal force either in the compression and tension zone
δ_s	-	Interface slip
σ_n	-	Stress per unit area caused by the external normal force across the interface that can act simultaneously with the shear force
τ	-	Interface shear strength
τ_{calc}	-	Calculated interface shear strength
τ_{exp}	-	Experimental interface shear strength
τ_u	-	Ultimate shear stress from the cross section area
τ_c	-	Concrete cohesion strength, adhesion
τ_{FEM}	-	Finite element modeling interface shear strength
V	-	Applied shear force at location under consideration
V_{FEM}	-	Ultimate shear capacity from FEM
V_{calc}	-	Calculated ultimate shear capacity
V_u	-	Total ultimate shear force
ρ	-	Steel ratio
A_s	-	Total cross-sectional area of the steel reinforcement crossing the interface
A_g	-	Cross section area of the interface

μ	-	Friction coefficient
f_{cd}	-	Design value of concrete compressive strength
f_c	-	Compressive strength of concrete
f_{ck}	-	Compressive strength of concrete (cylinder strength)
f_{ct}	-	Concrete tensile strength
f_{cu}	-	Concrete compressive cube strength
f_{yd}	-	Design tensile strength of the shear reinforcement
f_y	-	Yield strength of the steel reinforcement
h	-	Full depth of the section
h_c	-	Depth to the centroid of core from the top of the composite section
h_t	-	Depth of concrete topping
h_s	-	Depth of precast concrete
s	-	Spacing of shear reinforcement
v	-	Poisson's ratio of concrete
w_d	-	Uniform load distribution
x	-	Distance from the top of concrete topping to the neutral axis of the transformed composite section
x_u	-	Centroid from the top of the composite section of the uncracked section
A_s	-	Area of the tension reinforcement
${A_s}'$	-	Area of the compression reinforcement
y_s	-	Distance from the neutral axis of the composite section to the steel centroid
y_t	-	Distance from the neutral axis of the composite section to half of the concrete topping depth
z	-	Lever arm of the composite section
A_c	-	Cross section area of precast section

A_{comp}	-	Cross section area of the composite section
A_i	-	Area of reinforcement crossing the interface
E_{base}	-	Elastic modulus of the concrete base
$E_{topping}$	-	Elastic modulus of the concrete topping
E_s	-	Elastic modulus of the steel reinforcement
I	-	Second moment of area
I_u	-	Second moment of area of the uncracked section
I_{u2}	-	Second moment of area of the uncracked composite section
L	-	Effective length between the support
M	-	Applied imposed bending moment
N	-	Magnitude of the resultant normal force
P	-	Applied imposed load
F	-	Tensile force applied at the centroid of the concrete topping to overcome the strain differential between the concrete topping and precast slab
F_R	-	Resultant force of the stress distribution
d	-	Effective depth of the tension reinforcement
d'	-	Effective depth of the compression reinforcement
a	-	Shear span
c	-	Concrete cohesion, cohesion coefficient
C	-	Concrete cohesion strength
b_i	-	Interface width
η_d	-	Design action
q_k	-	Characteristic variable action
g_k	-	Characteristic permanent action
K_s	-	Shear stiffness
l_m	-	Sampling length

κ	-	Interaction “effectiveness” factor
δ	-	Displacement, separation
T	-	Traction
T_{max}	-	Maximum traction
G_c	-	Fracture toughness, critical energy release rate
G_{TC}	-	Fracture energy
K_s	-	Shear stiffness
t_n	-	Normal traction
t_s	-	Transverse traction (mode II)
t_t	-	Transverse traction (mode III)
t_n^0	-	Nominal tensile
t_s^0	-	Shear strength (mode II)
t_t^0	-	Shear strength (mode III)
η	-	BK material parameter
G_{IC}	-	Fracture energy (mode I)
G_{IIC}	-	Fracture energy (mode II)
G_{IIIC}	-	Fracture energy (mode III)
S	-	Peak shear load
δ_s^{init}	-	Initial displacement at maximum peak shear load (damage iniation)
δ_s^{fail}	-	Failure displacement at fracture
F_s	-	Drucker-Prager failure surface
β	-	Material angle of friction
d	-	Cohesion in the p-t plane
R	-	Cap eccentricity parameter
c	-	Material cohesion
f_s	-	Average stress of steel bars

ε_s	-	Average strain of steel bars
f_y	-	Yield stress of bare steel bars
ε_y	-	Yield strain of bare steel bars
V_{ult}	-	Ultimate shear strength capacity
δ	-	Deflection at ultimate shear strength capacity
δ_s	-	Interface slip at ultimate shear strength capacity
V_{Edi}	-	Transverse shear force
ν_{Edi}	-	Design value of the shear stress at the interface
ν_{Rdi}	-	Design shear resistance at the interface
t_i	-	Initial time
R_a	-	Average roughness
R_z	-	Mean peak-to-valley height
R_{max}	-	Maximum peak-to-valley height
R_{3z}	-	Mean third highest peak-to-valley height
$R_{3z_{max}}$	-	Maximum third highest peak-to-valley height
R_y	-	Total roughness height
R_{pm}	-	Mean peak height
R_p	-	Maximum peak height
R_{vm}	-	Mean valley depth
R_v	-	Maximum valley depth
R_q	-	Root-mean-square (RMS) profile height
R_{sk}	-	Skewness of the assessed profile
R_{ku}	-	Kurtosis of assessed profile
R_t	-	Total peak-to-valley height
n	-	Number of measured points

LIST OF ABBREVIATIONS

ACI	-	American Concrete Institute
CEB	-	Comité Euro-International du Béton
CDP	-	Concrete Damaged Plasticity
CPM	-	Modified Drucker-Prager/Cap Plasticity Model
CZM	-	Cohesive Zone Model
FEM	-	Finite Element Modeling

LIST OF APPENDICES

APPENDIX	TITLE	PAGE
A	Design of Composite Slab	280
B	Determination of Interface Shear Strength Based on the Proposed Method by Gohnert and ACI’s Alternative Theory	283
C	Analysis and Design of Composite Slab	288
D	List of Publications	290

CHAPTER 1

INTRODUCTION

1.1 Introduction

Precast slab is widely used in reinforced concrete building, such as in offices, condominiums, hotels, commercial buildings, educational facilities and even high-rise buildings. For precast slab, they have the ability to cover large span area apart from other advantages such as comparatively low weight and reduced construction time. Furthermore, the use of formwork is minimal due to its flexibility in design. Precast slab composed of a singular unit, which is cast at the factory, transported and erected at the construction site as shown in Figure 1.1.

Figure 1.1 Placing the precast slab

After placing each unit of the precast slab, they are joined together by grouting along its longitudinal joints. In order to enhance the structural performance of the precast slab, cast in-place topping is added to produce a completed floor finishes. The added concrete topping increases the slab thickness which contributes to higher flexural and shear strength. However, it is essential to produce adequate interface shear stress along the contact between the precast slab and concrete topping.

As mentioned in the Code of Practice (ACI 318, 2008; Eurocode, 2004 and CEB-FIB Model Code 2010, 2010), interface shear strength between an existing concrete base and concrete topping must be maintained through concrete cohesion, friction and dowel action from the projecting steel reinforcement. For the surface without the projecting steel reinforcement, interface shear depends on the surface roughness contributing from the concrete cohesion and friction coefficient. Figure 1.2 shows the forces acting on the composite slab and flexural strain distribution between the concrete base and concrete topping.

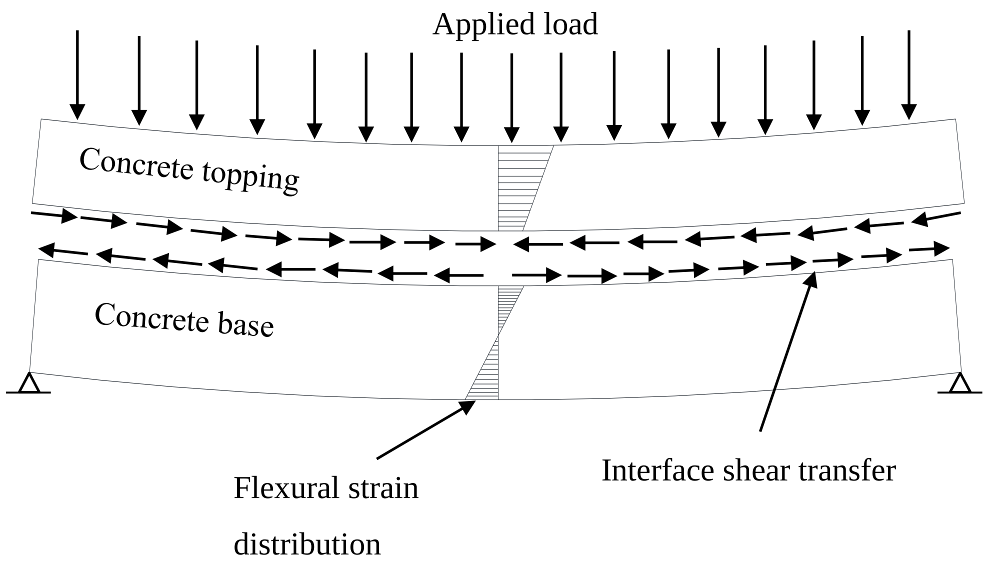

Figure 1.2 Composite action between existing precast slab and newly added concrete topping

1.2 Problem Statement

Most previous studies when quantifying the interface shear strength of interface concrete with projecting steel, concrete cohesion is not taken into consideration. They only considered friction from the normal stress and clamping stress. Similarly, interface concrete without projecting steel which depended solely on the surface texture considered only concrete cohesion in quantifying the interface shear strength. Although there are little studies conducted on the action due to the variable normal stresses, however, the findings still lack for the various surface textures which considered smooth or left “as-cast” as the only type of surface by the previous researcher. So far no research has been conducted on concrete layers with variable normal stresses and different types of surface textures at the interface with and without the projecting steel. Furthermore, Finite Element Modeling (FEM) of the interface shear behavior for concrete-to-concrete bond is also lacking in research. New interface modelling technique is introduced in this study for different surface textures.

The addition of the cast-in place topping increases the flexural and shear strength of composite slab by increasing the effective depth. This additional parameter can increase the service and ultimate load of the composite slab. It is important for the composite slab that the interface transfers all stresses sufficiently and without any slippage. The flexural strength of the composite slab may reduce if the components are not acting monolithically. If the loading system exceeded the interface shear strength capacity, the precast slab and concrete topping will begin to slide relative to each other. The situations where the interface shear strength exceeded the design strength, projecting steels are added on the top surface of the precast as shown in Figure 1.3. This projecting steel crosses the interface will give additional bond and therefore increases the interface shear strength capacity. Furthermore, the projecting steel is added to resist further interface slip to occur and maintained the integration between the precast slab and concrete topping.

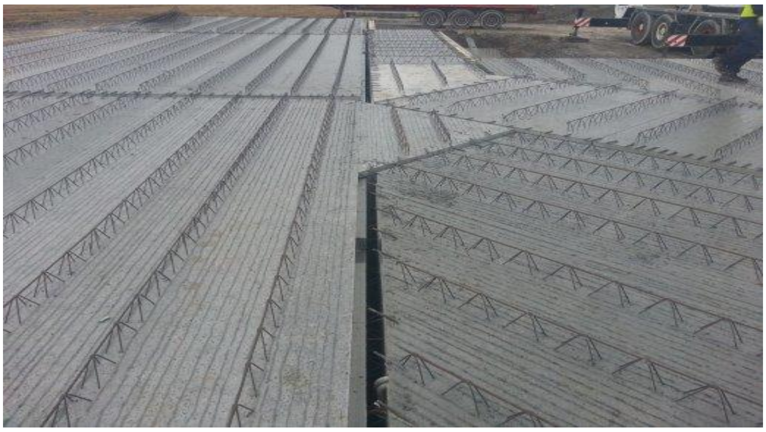

Figure 1.3 Projecting steel at the top of the precast slab

In order for the composite slab to behave monolithically, the bond at the interface between the precast slab and concrete topping must remain intact. The interface shear stress must be sufficiently transferred along the interface of the two concretes. However, when load is applied on the weaker interface bond, it may cause interface failure due to slippage of the concrete topping. If this slip occurred and the composite action is lost, only friction force is acted between the precast slab and concrete topping. Therefore, each concrete layers will deform separately due to the vertical forces which causes tension at the bottom of the two concretes. Figure 1.4 and 1.5 show the stress distributions for the weak interface bond (non-composite section) and the strong interface bond (composite section) of the composite slab.

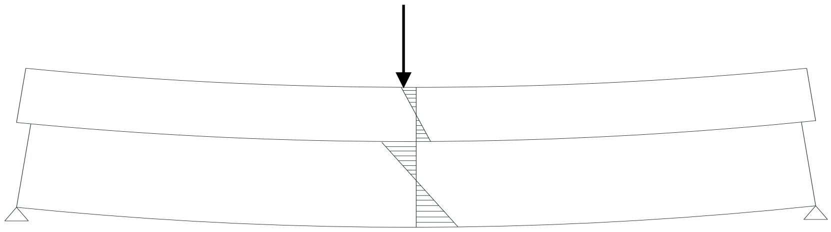

Figure 1.4 Non-composite section **(**Kovach and Naito, 2008)

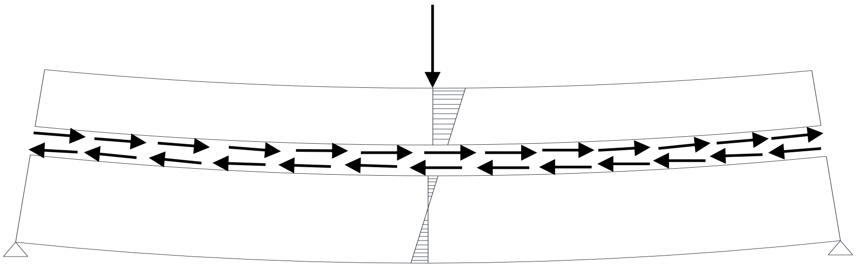

Figure 1.5 Composite section **(**Kovach and Naito, 2008)

The “shear-friction theory” is adopted in major Codes of Practice to predict the interface shear strength between concrete layers cast at different times. The “shear-friction theory” considers the interface shear stress must be transferred crossing the interface of concrete layers and simultaneously subjected to external normal stress that causes friction. The following interface shear strength parameters are considered; (a) compressive strength of the weakest concrete; (b) normal stress acted at the interface; (c) projecting steel crossing the interface; and (d) surface texture on the top surface of the concrete base.

1.3 Objectives

The objectives of this study are as follows:

i. To evaluate the interface shear strength of composite slab with different surface textures using the “push-off” test method.
ii. To determine the relationship of the interface shear strength considering the contribution of the friction coefficient, concrete cohesion, normal stress and clamping stress from projecting steel.

iii. To determine the interface shear strength of Finite Element Modeling on the composite slab with different surface textures and to compare the result from the "push-off" test method.

iv. To determine the relationship of the interface shear strength to the shear capacity of the full scale composite slab from the Finite Element Modeling.

1.4 Scope of Study

This study focused on the interface shear strength between existing concrete base and newly cast in-situ concrete topping. The background information of the interface shear strength quantification methods in the current design codes is described in Chapter 2.

To investigate the effect on the interface shear strength considering friction coefficient, concrete cohesion, dowel action from the projecting steel reinforcement and surface preparation specified in Eurocode 2 (2004), experimental work is carried out on small-scale specimens. The "push-off" test method is carried out to study the influence of different surface textures on the interface shear strength. The top surfaces of the concrete base are treated in six different ways:

(a) smooth or "left as-cast" with trowelled finish,
(b) deep groove formed using a 16 mm steel bar,
(c) roughened by wire-brushing in the longitudinal direction,
(d) roughened by wire-brushing in the transverse direction,
(e) indented surface cast using a corrugated steel mold, and
(f) projecting steel reinforcement crossing the interface.

The surface with projecting steel reinforcement is to make comparison with the other surfaces without any steel reinforcement. The roughness of each texture is measured using a Portable Stylus instrument to quantify the roughness parameters to determine the relationship between interface shear strength and surface roughness.

For each of surface texture, concrete topping of 300 × 300 × 75 mm deep is cast on top of the 300 × 300 × 100 mm deep concrete base. Loading is applied simultaneously in two directions; horizontally along the interface and vertically with variable normal stresses. The variable normal stresses are applied at 0.5 N/mm^2, 1.0 N/mm^2 and 1.5 N/mm^2 for each specimen in order to define the Mohr-Coulomb failure envelope.

In the finite element modeling, small-scale models are developed using ABAQUS. For verification purposes, the finite element modeling results are compared with the “push-off” test results. All material properties and design parameters are the same with the “push-off” test specimens. The finite element results will give a thorough insight on the interface shear failure criterion, elastic stiffness and fracture energy that influence the interface shear failure.

To verify the small-scale models, full-scale composite slab specimens are also modeled using finite element method. The slab is one-way, simply supported and restrained at both ends. The dimension of each layer is 3000 mm length × 1200 mm width. Meanwhile, the thickness of the base is 100 mm and concrete topping is 75 mm. The material properties and design parameters are the same with the small scale modeling.

1.5 Significant of Study

This study gives clear understanding on the influence of different types of surface texture on the interface shear strength of the composite slab. The interface shear strength empirical equation proposed in this study takes into account the roughness depth, friction and concrete cohesion. Moreover, as the research show that the surface without projecting steel can be put greater reliance on the friction and concrete cohesion then it is possible to reduce or even eliminate the use of projecting steel. The significant findings of this research will be beneficial in the following ways:

i. Aid in suggesting the friction and concrete cohesion values in Eurocode 2 based on quantification of surface textures which will provide accurate prediction and replace the qualitative observation on surface textures.
ii. Assist fabricators and engineers in improving the quality of surface preparation for precast construction and providing an established database for design works in the future.
iii. The reduction of projecting steel crossing the interface can reduce the fabrication cost thus reducing the time to bend and tied the steel.
iv. Provide construction safety in which the presence of projecting steel on top of the precast slab can exposed tripping hazard to the safety of workers.
v. The study will provide a FE model of simplified “push-off” specimens that can accurately represent the shear transfer at concrete-to-concrete bond. This model can be used for predicting the interface shear strength as well as slip with varied parameters.

1.6 Thesis Organization

The structure of this thesis is as follows:

(a) Chapter 2 presents the literature review on the subject of this thesis.

(b) Chapter 3 describes the test setup and instrumentation used in the experimental work for the small-scale “push-off” test specimens.

(c) Chapter 4 describes the Finite Element modeling technique of the small-scale and full-scale specimens.

(d) Chapter 5 presents the experimental results and analysis of the small-scale "push-off" test. Analytical work on the proposed expression for the interface shear strength is also presented in this chapter.

(e) Chapter 6 presents the Finite Element modeling results of the small-scale specimens. The comparison and verification with the experimental "push-off" test results are also discussed in this chapter.

(f) Chapter 7 presents and discussed the Finite Element modeling results of the full-scale composite slab.

(g) Chapter 8 presents the conclusion of all the test results and recommendation for further study.

(projecting steel surface), 0.53 N/mm^2 (indented surface) and 0.91 N/mm^2 (transverse roughened surface).

iii. The highest interface shear strength is found at transverse roughened surface as higher interface shear strength property is applied compared to other surface textures. This then followed by indented, projecting steel and smooth surfaces. The interface shear strength at projecting steel surface is lower than indented surface even though higher vertical shear strength is found at projecting steel surface compared to indented surface. Due to stress transfer from interface layer to the projecting steel, deformation at projecting steel is occurred.

iv. The same interface shear strength properties are applied to both of small-scale and full-scale of FE modeling and the values from full-scale of composite slab is smaller than the small-scale of experimental and finite element. This is due to different size and configuration between the specimen models that give different result. The study concluded that the design interface shear strength, v_{Rdi} from the proposed equation of the "push-off" test should be higher than the interface shear strength, v_{Edi} based on the ultimate vertical shear load of the full-scale FE model of composite slab. As stated in Eurocode 2, the actual interface shear strength should be lower or equal to the design value ($v_{Edi} \leq v_{Rdi}$) for the composite slab to act monolithically.

8.2 Recommendations for Further Investigations

The areas for further studies that are essential for adequate information on the interface shear strength are suggested as follows:

i) Further experimental research focusing on the quality of surface preparation such as the removal of concrete laitance would provide more detailed insight on the effect to the interface shear strength. Concrete laitance can be found on existing concrete due to cutting during the precast slab production. Therefore, building defects can be prevented prior to the construction work.

ii) Further experimental work involving the provision related to the curing conditions, differential shrinkage and stiffness between concrete base and concrete topping.

iii) Experimental study on the full-scale composite concrete slab should be further conducted on bending and combination of shear-bending tests.

REFERENCES

ACI Committee 318. (2008). *Building code requirements for structural concrete (ACI 318M-08) and commentary*. American Concrete Institute, Farmington Hills, MI.

Alfano, G. (2006). On the influence of the shape of the interface law on the application of cohesive-zone models. *Composites Science and Technology*. 66(6), 723-730.

Anderson, A.R. (1960). Composite Designs in Precast and Cast-in-Place Concrete. *Progressive Architechture*. 41(9), 172–179.

Aysen, A. *Soil mechanics: basic concepts and engineering applications*. Swets & Zaitlinger B. V., Lisse, The Netherlands: A. A. Balkema Publishers. 2005.

Baldwin, M. I. and Clark L. A. (1997). Push-off shear strength with inadequately anchored interface reinforcement. *Magazine of Concrete Research.* 48(178), 35-43.

Barenblatt, G. (1962). The mathematical theory of equilibrium cracks in brittle fracture. *Advanced Applied Mechanics*. 7, 55-129.

Bass, R. A., Carrasquillo, R. L., and Jirsa, J. (1990). Shear Transfer across New and Existing Concrete Interfaces. *ACI Structural Journal.* 86, 383-393.

Birkeland, H. and Birkeland, P. (1966). Connections in Precast Concrete Construction. *Journal of American Concrete Institute*. 63(3), 345-368.

Biscaia, H.C., Chastre, C., and Silva, M. A. G. (2012). Double shear tests to evaluate the bond strength between GFRP/concrete elements. *Composite Structures*. 94(2), 681-694.

BSI Standards Publication. *Assessment of surface texture – Guidance and general information*. London, BS 1134. 2010.

Borst, D., Remmers, J. J. C. and Needleman, A. (2006). Mesh-independent discrete numerical representations of cohesive-zone models. 73, 160-177.

Courard L. and Nelis M. (2003). Surface analysis of mineral substrates for repair works: roughness evaluation by profilometry and surfometry analysis. *Magazine of Concrete Research.* 55(4) 355-366.

Deaton, J. (2005). *A Finite Element Approach to Reinforced Concrete Slab Design*. Master Thesis. Georgia Institute of Technology.

Dias-da-Costa, D., Alfaiate, J., and Júlio, E. N. B. S. (2012). FE modeling of the interfacial behaviour of composite concrete members. *Construction and Building Materials*. 26(1), 233-243.

Dugdale, D. S. (1960). Yielding of steel sheets containing slits. *Journal of the Mechanics and Physics of Solids*. 8, 100-104.

Espeche A. D. and León, J. (2011). Estimation of bond strength envelopes for old-to-new concrete interfaces based on a cylinder splitting test. *Construction Building Material*. 25(3), 1222-1235.

Eurocode 2 (2004). Design of concrete structures – Part 1: General rules and rules for buildings. *EN 1992-1-1*. Avenue Marnix 17, B-1000 Brussels, Belgium: European Committee for Standardization.

Ferracuti, B., Savoia, M., and Mazzotti, C. (2007). Interface law for FRP–concrete delamination. *Composite Structures*. 80(4), 523-531.

Gadelmawla E. S., Koura M. M., Maksoud T. M. A. and Elewa I. M. (2002). Roughness parameters. *Journal Material Process Technology*. 123, 133-145.

Gohnert, M. (2000). Proposed theory to determine the horizontal shear between composite precast and in situ concrete. *Cement and Concrete Composites*. 22, 469-476.

Gohnert, M. (2003). Horizontal shear transfer across a roughened surface. *Cement and Concrete Composites.* 25, 379-385.

Hadjazi, K., Sereir, Z., and Amziane, S. (2012). Cohesive zone model for the prediction of interfacial shear stresses in a composite-plate RC beam with an intermediate flexural crack. *Composite Structures*. 94(12), 3574-3582.

Hanson, N. W. (1960). Precast-prestressed concrete bridges. 2. Horizontal shear connections. *Development Department Bulletin D35. Portland Cement Assoc*, 2(2), 38-58.

Hofbeck, J. A., Ibrahim I. O., and Mattock, A. H. (1969). Shear Transfer in Reinforced Concrete. *ACI Journal*. 66, 119-128.

Ibrahim, I. S. (2008). *Interface Shear Strength of Hollow Core Slabs with Concrete Toppings*. Ph.D. Thesis. The University of Nottingham.

Ibrahim, I. S., Elliott, K. S. and Copeland, S. (2008). Bending Capacity of Precast Prestressed Hollow Core Slabs wih Concrete Toppings. *Malaysian Journal of Civil Engineering*. 20(2), 260-283.

Ingraffea, A. R., Gerstle, W. H., Gergely P. and Souma, V. (1984). Fracture mechanics of bond in reinforced concrete. *Journal of Structural Engineering*. 110(4), 871-890.

Joshani, M., Koloor, S. S. R., and Abdullah, R. (2012). Damage Mechanics Model for Fracture Process of Steel-concrete Composite Slabs. *Applied Mechanics and Materials*. 165, 339-345.

Júlio, E. N. B. S., Branco, F. A. B., Silva, V. D., and Lourenco, J. F. (2006). Influence of added concrete compressive strength on adhesion to an existing concrete substrate. *Building and Environment*. 41(12), 1934-1939.

Júlio, E. N. B. S., Branco, F. A. B., and Silva, V. D. (2004). Concrete-to-concrete bond strength. Influence of the roughness of the substrate surface. *Construction and Building Materials*, 18(9), 675-681.

Júlio, E. N. B. S., Branco, F. A. B., and Silva, V. D. (2005). Concrete-to-concrete bond strength: influence of an epoxy-based bonding agent on a roughened substrate surface. *Magazine of Concrete Research.* 57, 1-6.

Kaar, P. H., and Mattock, A. H. (1961). Precast-prestressed concrete bridges. 4. Shear tests of continuous girders. *Journal of PCA Research & Development Laboratories*. 3(1), 19-46.

Kahn, L. F. and Mitchell A. D. (2002). Shear friction tests with high-strength concrete. *ACI Structural Journal*. 99(1), 98-103.

Kaliakin, V. N. and Li, J. (1995). Insight into deficiencies associated with commonly used zero-thickness interface elements. *Computers Geotechnics*, 17(2), 225-252.

Karabinis, A. I. and Rousakis, T. C. (2002). Concrete confined by FRP material: A plasticity approach. *Engineering Structures*, 24(7), 923-932.

Kovach, J. D. and Naito, C. (2008). Horizontal Shear Capacity of Composite Concrete Beams without Interface Ties. *ATLSS Report No. 08-05.*

Koh, Y. K. (2011). *Characterizing A Reinforced Concrete Beam-Column-Slab Subassemlage Connection for Progressive Collapse Assessment*. Ph.D Thesis. University of Florida, USA.

Lavenhagen, D. M. (2012). *A Numerical Assessment of Direct Shear Behavior in Concrete.* Master Thesis. University of Florida, USA.

Loov, R. E. and Patnaik, A. K. (1994). Horizontal shear strength of the composite beam with rough interface. *PCI Journal*, 39(1), 48-69.

Malm, R. (2009). *Predicting shear type crack initiation and growth in concrete with non- linear finite elemetn method*. Ph.D Thesis. Royal Institute of Technology, Stockholm, Sweden.

Mansour, F. R., Abu Bakar, S., Ibrahim, I. S., Marsono, A. K. and Marabi, B. (2015). Flexural performance of a precast concrete slab with steel fiber concrete topping. *Construction & Building Materials*. 75, 112-120.

Mansur, M. A., Vinayagam, T., and Tan, K. W. (2008). Shear Transfer across a Crack in Reinforced High-Strength Concrete. *Journal of Materials in Civil Engineering, ASCE.* 20, 294-302.

Mast, R. F. (1968). Auxiliary reinforcement in precast concrete connections. *ASCE J Struct Div*. 94(6), 1485-1504.

Mattock A. H. and Hawkins, N. (1972). Shear transfer in reinforced concrete – recent research. *PCI Journal*. 17(2), 55-75.

Mattock A. H. and Kaar, P. H. (1961). Precast-Prestressed Concrete Bridges 4. Shear Tests of Continous Girders. Development Department Bulletin D45, Portland Cement Association. 19-47.

Mattock A. H. (1988). Reader comments of paper 'Influence of concrete strength and load history on the shear friction capacity of concrete members' published in PCI Journal, January–February 1987;32(1):66-84, by Walraven J, Frénay J, Pruijssers A. *PCI J 1988*, 33(1), 165-166.

Model Code 2010 (2010). *Comité Euro-International du Béton, Secretariat Permanent, First complete draft.* International Federation for Structural Concrete (*fib*). Case Postale 88, CH-1015 Lausanne, Switzerland.

Mokhatar, S. N. and Abdullah, R. (2012). Computational Analysis of Reinforced Concrete Slabs Subjected to Impact Loads. *International Journal of Integrated Engineering.* 4(2), 70-76.

Momayez A., Ehsani M. R., Ramezanianpour A. A., and Rajaie H. (2005). Comparison of methods for evaluating bond strength between concrete substrate and repair materials. *Cement and Concrete Research*. 35(4), 748-757.

Mones, R. M. (2012). *Interfacial Strength Between Prestressed Hollow Core Slabs and Cast-In-Place Concrete Topping*. Master Thesis. University of Massachusetts Amhert.

Neto, P., Alfaiate, J., Almeida, J. R. and Pires, E. B. (2004). The influence of mode II fracture on concrete strengthened with CFRP. *Computers & Structures*, 82, 17-19.

Neto, P., Alfaiate, J., Almeida, J. R. and Pires, E. B. (2004). The influence of the mode II fracture energy on the behaviour of composite plate reinforced concrete. *Proceedings FraMCoS-5,* Vail, Colorado. USA,781-786.

Nielsen, M. P. and Hoang, L. C. *Limit Analysis and Concrete Plasticity*. (3rd ed.) Rosewood Drive, Danvers: Taylor and Francis Group. 2011.

Pan, J. and Wu, Y. F. (2014). Analytical modeling of bond behavior between FRP plate and concrete. *Composites Part B: Engineering*. 61, 17-25.

Papanicolaou, C.G. (2002). Shear transfer capacity along pumice aggregate concrete and high-performance concrete interfaces. *Materials and Structures*, 35, 237-245.

Patnaik, A. K. (1999). Longitudinal Shear Strength of Composite Concrete Beams with a Rough Interface and no Ties. *Australian Journal of Structural Engineering*. 3(SE1), 157-166.

Patnaik, A. K. (2001). Behavior of Composite Concrete Beams with Smooth Interface. *Journal of Structural Engineering*, 127, 359-366.

Perales, F., Dubois, F., Monerie, Y., Piar, B. and Stainier, L. (2010) Multi-body nscd strategyas a multi-domain solver. application to code coupling dedicated to the modeling of fracture of heterogeneous media. *European Journal of Computational Mechanics*. 19, 189-417.

Perez, F., Morency, M., and Bissonnette, B. (2009). Correlation between the roughness of the substrate surface and the debonding risk. *Concrete Repair, Rehabilitation and Retrofitting II*. 949-956.

Revesz, S. (1953). Behavior of Composite T-Beams with Prestressed and Unprestressed Reinforcement. *ACI Journal*. 24(6), 585-592.

Richefeu, V., Chrysochoos, A., Huon, V., Monerie, Y., Peyroux, R. and Wattrisse, B. (2012). Toward local identification of cohesive zone models using digital imagecorrelation. *European Journal of Mechanics A/Solids.* 34, 38-51.

Ros, P. (1994). Experimental Research on Prestressed Hollow Core Slabs Floors with Insitu Concrete Topping. *FIP 12th International Congress.* Washington: Federation Internationale de la Precontraine.

Saemann, J. C. and Washa, G. W. (1964). Horizontal Shear Connections Between Precast Beams and Cast-in-Place Slabs. *ACI Journal*. 61(11), 1383-1409.

Santos, P. M. D., Júlio, E. N. B. S. and Silva, V. D. (2007). Correlation between concrete-to-concrete bond strength and the roughness of the substrate surface. *Construction and Building Materials*. 21(8), 1688-1695.

Santos, P. M. D. and Júlio, E. N. B. S. (2010). Effect of Filtering on Texture Assessment of Concrete Surfaces. *ACI Materials Journal*. 107, 31-37.

Santos, P. M. D. and Júlio, E. N. B. S. (2011). Comparison of Methods for Texture Assessment of Concrete Surfaces. *Journal of American Concrete Institute*. 107, 433-440.

Santos, P. M. D. and Júlio, E. N. B. S. (2012). A state-of-the-art review on shear-friction. *Engineering Structures,* 45, 435-448.

Santos, D. S., Santos, P. M. D. and Dias-da-Costa, D. (2012). Effect of surface preparation and bonding agent on the concrete-to-concrete interface strength. *Construction and Building Materials*. 37, 102-110.

Santos, P. M. D. and Júlio, E. N. B. S. (2013). A state-of-the-art review on roughness quantification methods for concrete surfaces. *Construction and Building Materials*. 38, 912-923.

Santos, P. M. D. and Júlio, E. N. B. S. (2014). Interface Shear Transfer on Composite Concrete Members. *ACI Structural Journal*. 111, 113-121.

Scott, J. (2010). *Interface shear strength in lightweight concrete bridge girders*. Master Thesis. Virginia Polytechnic Institute and State University.

Scott, N. L. (1973). Performance of Precast Prestressed Hollow Core Slab with Composite Concrete Topping. *PCI Journal*, 18(2), 64-77.

Shin D., Lee H., and Cho C. (2007). Computational Study on Mechanical Behavior of Steel-concrete Composite by using Interface Elements. *Key Engineering Materials*. 346, 909–912. Trans Tech Publications.

Simulia. (2012). *Abaqus version 6.12 documentation*. Dassault Systèmes Simulia Corporation.

Sonnenberg, A. M. C., Al-Mahaidi, R., and Taplin, G. Ã. (2003). Behaviour of concrete under shear and normal stresses. *Magazine of Concrete Research*. 4, 367-372.

Swedish Standard. *Concrete surfaces – determination surface roughness*. Ed. Stockholm, SIS 81 20 05. 1981.

Taylor R. (1990). Interpretation of the correlation coefficient : A basic review. *Journal Diagnostic Medical Sonography*. 6(1), 35-39.

Wallenfelsz, J. A. (2006). *Horizontal shear transfer for full-depth precast concrete bridge deck panels*. Master Thesis. Virginia Polytechnic Institute and State University.

Walraven, J., Frenay, J. and Pruijssers, A. (1987). Influence of Concrete Strength and Load History on the Shear Friction Capacity of Concrete Members. *PCI Journal*. 32(1), 166-184.

Wang, J. (2007). Cohesive-bridging zone model of FRP – concrete interface debonding. *Engineering Fracture Mechanics*. 74, 2643-2658.

Wang, T. and Hsu, T. T. C. (2001). Nonlinear finite element analysis of concrete structures using new constitutive models. *Computers & Structures*. 79, 2781-2791.

Wong, R. C. K., Ma, S. K. Y., Wong, R. H. C., and Chau, K. T. (2007). Shear strength components of concrete under direct shearing. *Cement and Concrete Research.* 37, 1248-1256.

Zilch K. and Reinecke R. (2000). Capacity of shear joints between high-strength precast elements and normal-strength cast-in-place decks. *fib International symposium on high performance concrete*. 25-27 September 2000. Orlando, USA, 1-10.